An Investigation of Secondary Ion Yield Enhancement Using Bi_n^{2+} (n = 1, 3, 5) Primary Ions

Gabriella Nagy, Peng Lu, and Amy V. Walker
Department of Chemistry, Washington University in St. Louis, St. Louis, Missouri, USA

We have investigated secondary ion yield enhancement using Bi_n^{2+} (n = 1, 3, 5) primary ions impacting phenylalanine, 1,2-dipalmitoyl-*sn*-glycero-3-phosphocholine (DPPC), 1,2-dipalmitoyl-*sn*-glycero-3-phosphoethanolamine (DPPE), cholesterol, Irganox 1010, and polymer films adsorbed on silicon and aluminum. Secondary ion yields are increased using Bi^{2+} and Bi_3^{2+} primary ions for the molecular layers and polymers that can undergo allyl cation rearrangements. For Irganox 1010, the deprotonated molecular ion yields (*m/z* 1175; $[M - H]^-$) are one to two times larger for Bi^{2+} and Bi_3^{2+} primary ions than for Bi^+ and Bi_3^+ at the same primary ion velocities. In the positive ion mode, the largest fragment ion yield (*m/z* 899) is ~1.5 times larger for Bi^{2+} ions than for Bi^+. For Bi_3^{2+} the largest fragment ion yield is only ~70% of the ion yield using Bi_3^+, but the secondary ion yields of the fragment ions at *m/z* 57 and 219 are enhanced. For polymers that can undergo allyl cation rearrangement reactions the secondary ion yield enhancements of the monomer ions range from 1.3 to 4.3. For Bi_5^{2+} primary ions, secondary ion yields were the same or slightly larger than for Bi_5^+ in the negative ion mass spectra for Irganox 1010, but lower in the positive ion mode. No secondary ion yield enhancements were measured on polymer samples for Bi_5^{2+}. For all polymer films studied, secondary ion intensities from the oligomer regions are substantially decreased using Bi_n^{2+} (n = 1, 3, 5). We discuss differences in the ionization mechanisms for doubly and singly-charged Bi primary ion bombardment. (J Am Soc Mass Spectrom 2008, 19, 33–45) © 2008 American Society for Mass Spectrometry

Secondary ion mass spectrometry (SIMS) has many applications in areas such as microelectronics, geology, biotechnology, and materials science [1, 2]. SIMS is used to obtain both atomic- and molecular-specific images of samples with submicron resolution and depth profiles. The utility of SIMS has been greatly increased recently by the introduction of polyatomic primary ion beams [2, 3]. Polyatomic projectiles, such as Bi_n^+ [4–6] and Au_n^+ [7–13], have been demonstrated to greatly enhance molecular ion yields compared to monoatomic primary ions such as Ga^+ or Ar^+. The use of polyatomic primary ions has also led to improvements in the useful lateral resolution of SIMS mass spectrometric (chemical) images [5].

In a typical SIMS experiment, the primary ions are singly charged and have kinetic energy in the 2 to 50 kiloelectronvolt (keV) range. They transfer energy and momentum to atoms in the sample, which are displaced from their original position and ejected into the vacuum [1, 2]. For multiply charged primary ions there is a second possible interaction known as potential sputtering [14]. In addition to kinetic energy, primary ions also carry potential energy that can be large if the ion is highly charged. This potential arises when q electrons are removed from species A to create an A^{q+} ion. For highly charged ions, such as Ar^{9+}, this potential can be in the keV range [14]. When such an ion strikes the surface, it induces a variety of nonelastic processes within the sample. These processes lead to the removal of atoms and ions from the sample surface. The use of highly-charged primary ions has been demonstrated to greatly enhance the ion yields from surfaces. For example, below $q \sim 25$ the secondary ion yield from silicon surfaces increases linearly with incident (primary) ion charge. However, above this threshold, the secondary ion yields from silicon surfaces increases nonlinearly with the primary ion charge above q ~25 [14].

There have been a few reports of nonlinear yield enhancement using multiply charged primary ions with $q < 25$. Schweikert et al. observed that in 18 keV Ar^{q+} ($1 \leq q \leq 11$) bombardment of SiO_2, CsI, and phenylalanine films the secondary ion yields of H^+ ions were greatly enhanced by the use of multiply-charged ($q > 1$) Ar primary ions [15]. However, no other secondary ions were enhanced. Kakutani and coworkers demonstrated that Ar^{q+} and N^{q+} primary ion bombardments greatly enhanced the H^+, H_2^+ and H_3^+ ion yields from a C_{60} sample [16]. Further, these authors showed that the increase in the H^+ ion yield was due to potential sputtering and not nuclear

Address reprint requests to Dr. A. V. Walker, Department of Chemistry, Washington University in St. Louis, Campus Box 1134, One Brookings Drive, St. Louis, MO 63130, USA. E-mail: walker@wustl.edu

1044-0305/08/$32.00
doi:10.1016/j.jasms.2007.10.016

Published online October 30, 2007
Received May 4, 2007
Revised October 21, 2007
Accepted October 21, 2007

recoil. Benguerba et al. [7] observed that there was no increase in secondary ion yields from a *DL*-phenylalanine target using Au_n^{2+} (n = 1, 3) compared with Au_n^{+} (n = 1, 3) primary ions. However, more recently Walker and Winograd noted that the secondary ion yields of polystyrene oligomers were two to four times larger using Au^{2+} primary ions than using Au^{+} with the same primary ion velocity [8].

In this paper, we compare the secondary ion yields from thin organic films using Bi_n^{+} and Bi_n^{2+} (n = 1, 3, 5) primary ions at the same impact velocities. The films studied are used in a variety of important medical and technological applications. They include *DL*-phenylalanine, an amino acid, 2 phospholipids, 1,2-dipalmitoyl-*sn*-glycero-3-phosphocholine (DPPC), and 1,2-dipalmitoyl-*sn*-glycero-3-phosphoethanolamine (DPPE), cholesterol, and Irganox 1010, a common polymer additive. Polymers employed in this study are polystyrene (PS), polyethylene (PE), poly(2,6-dimethyl-p-phenylene oxide) (PDMPO), poly(propylene glycol) (PPG), polyisoprene (PI), poly(methyl methacrylate) (PMMA), polyethylene oxide (PEO), and polyethylene glycol (PEG). These compounds are shown in Structure **1**.

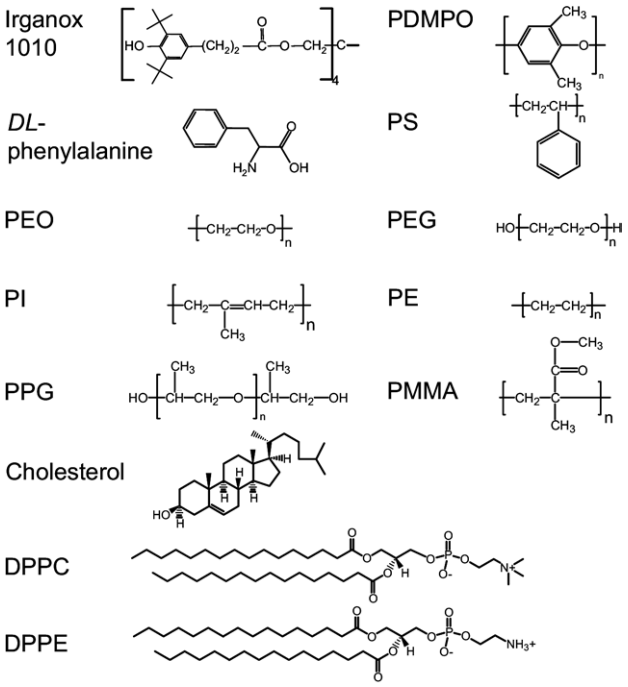

Structure 1. Structures of Irganox 1010, *DL*-phenylalanine, and polymers used in these studies.

These materials have all been previously characterized by SIMS, and *DL*-phenylalanine, Irganox 1010, and PS were used in previous studies of secondary yield enhancements using Bi_n^{+} [6] and Au_n^{+} primary ions [7, 8, 11, 13].

Using Bi_n^{2+} (n = 1, 3) primary ions the secondary ion yields increase for phenylalanine, DPPC, DPPE, cholesterol Irganox 1010, and for polymers that can undergo allyl cation rearrangements, PEO, PS, PPG, and PEG. In contrast, for PMMA, PTFE, and PDMPO no secondary ion yield enhancements were observed. For Bi_5^{2+} primary ions, secondary ion yields were the same or slightly larger in the negative ion mass spectra for Irganox 1010, but lower in the positive ion mode. No secondary ion yield enhancements were measured on polymer samples for Bi_5^{2+}. For all polymers studied, few or no oligomer ions were observed upon Bi_n^{2+} (n = 1, 3, 5) primary ion bombardment. Secondary ion yield enhancements were also found to vary with the preparation of the sample.

Experimental

Time-of-Flight Secondary Ion Mass Spectrometry

Time-of-flight secondary ion mass spectra were obtained using a TOF SIMS IV instrument (ION TOF Inc., Chestnut Ridge, NY). The instrument consists of a loadlock, a preparation chamber, and an analysis chamber, each separated by a gate valve. The preparation and analysis chambers were kept between 1×10^{-9} mbar and 5×10^{-9} mbar during experiments. The primary ion beam was generated using a liquid ion gun fitted with a pure Bi source capable of producing Bi_n^{x+} (n = 1, 3, 5; x = 1, 2) ions. The primary ions were mass selected by their flight time via a double blanking plate system. The kinetic energy of Bi_n^{+} and Bi_n^{2+} (n = 1, 3, 5) was 25 keV, so all the primary ions had the same velocity. The pulsed primary ion beam current was measured before and after obtaining a TOF SIMS spectrum using a Faraday cup (diameter ~ 2 mm), which is located on a grounded sample holder and using an extraction voltage of 2000 V to prevent emission of secondary electrons. The error in the primary ion beam measurement is very small and due to the loss of positive secondary ions (typically less than 1% of sputtered material is ionized [1]). The difference between the measured ion currents was ±5%, so any error in the primary ion beam measurement is smaller than the experimental error. Typical primary ion currents for a 25 kV singly-charged Bi primary ion beam are 1.0 pA (Bi^{+}), 0.35 pA (Bi_3^{+}), and 0.02 pA (Bi_5^{+}). Typical primary ion currents for a 12.5 kV doubly-charged Bi primary ion beam are 0.21 pA (Bi^{2+}), 0.035 pA (Bi_3^{2+}), and 0.02 pA (Bi_5^{2+}). The primary ion beam was bunched (compressed in time by a pulsed electric field) and had an initial pulse width of 30 ns. These ion beam conditions ensured sufficiently short pulses for TOF SIMS analysis with a mass resolution, $m/\Delta m$ ~ 5000 at m/z 29.

The secondary ions generated were extracted into a time-of-flight mass spectrometer using a potential of

Table 1. Positive ion secondary ion yields and yield enhancements for thin films of *DL*-phenylalanine adsorbed on silicon and aluminum using 25 keV Bi_n^{2+} and Bi_n^+ primary ions

	Y($C_8H_{10}N^+$; *m/z* = 120)		Y([M + H]$^+$; *m/z* = 166)	
Primary ion	Al	Si	Al	Si
Bi_3^+	4.4×10^{-3}	3.1×10^{-3}	8.3×10^{-4}	1.0×10^{-3}
Bi_3^{2+}	4.5×10^{-3}	3.9×10^{-3}	1.2×10^{-3}	7.5×10^{-4}
$Y(Bi_3^{2+})/Y(Bi_3^+)$	1.0	1.3	1.4	0.8
Bi^+	4.2×10^{-4}	2.7×10^{-4}	4.2×10^{-5}	1.6×10^{-4}
Bi^{2+}	5.1×10^{-4}	5.6×10^{-4}	4.8×10^{-5}	4.6×10^{-4}
$Y(Bi^{2+})/Y(Bi^+)$	1.2	2.1	1.1	2.9

2000 V. Before reaching the detector the secondary ions were reaccelerated to 10 kV.

Before analysis, preliminary measurements were taken to determine if there was any sample charging. The rate of detected ions was noted at the beginning and end of each experiment to ensure that there was no significant loss in data acquisition rate, which is indicative of sample charging. No evidence of sample charging was observed.

Analyzed areas were (152 × 152) μm^2 for all samples studied. The primary ion dose during data acquisition was less than 10^{10} ions·cm^{-2}, which is below the static SIMS limit [1]. Secondary ion peak intensities were reproducible to within ±5% from scan to scan. For samples prepared using spin-coating, secondary ion peak intensities were reproducible within ±15% from sample to sample. The secondary ion yield, Y, is defined as the number of secondary ions detected per incident primary ion. The number of secondary ions detected is corrected using Poisson statistics [17]. The secondary ion yields reported are averages from two different samples with at least three spots per sample analyzed (six measurements) except where noted. The error in the averaged secondary ion yields is ±20%.

Sample Preparation

Irganox 1010 was obtained from Ciba Specialty Chemicals (Tarrytown, NY), and cholesterol and *DL*-phenylalanine was from Sigma-Aldrich (St. Louis, MO). DPPC and DPPE were obtained from Avanti Polar Lipids, Inc. (Alabaster, AL). Narrow distribution polystyrene 771 (PS) (M_w = 1110), polyethylene (PE) (M_w = 1200), poly(2,6-dimethyl-p-phenylene oxide) (PDMPO) (M_w = 29,500), poly(propylene glycol) (PPG) (M_w = 2000), polyisoprene (PI) (M_w = 1000), poly(methyl methacrylate) (PMMA) (M_w = 20000), polyethylene oxide (PEO) (M_w = 25,000), and polyethylene glycol (PEG) (M_w = 1500) were obtained from Scientific Polymer Products, Inc. (Ontario, NY).

Irganox 1010, cholesterol, DPPC, DPPE, PDMPO, PEG, PMMA, PEO, PPG, PI, and PS were dissolved in chloroform as 1.00 mg/mL solutions. Polyethylene was dissolved in toluene as nominally 1.00 mg/mL solutions. A 10^{-2} M solution of *DL*-phenylalanine was prepared using a 1:1 2-propanol:water mixture as the solvent. Chloroform (high purity) and hexane were obtained from EMD Chemical, Gibbstown, NJ and from Burrick and Jackson, Muskegon, MI, respectively. Toluene (Sigma-Aldrich) and 2-propanol (Fisher Scientific, Pittsburgh, PA) were HPLC grade.

The substrates used were aluminum foil (99.99% purity, 0.1 mm thick, Alfa Aesar) and single crystal silicon wafer (κ orientation, Addison Engineering, San Jose, CA). Al foils were prepared by etching in 1:1 HNO_3:H_2O, rinsing several times in water, followed by rinsing in 2-propanol and drying with N_2 gas. The Si wafers were prepared using Piranha Etch (1:3 H_2O_2:H_2SO_4), followed by rinsing with copious amounts of water and 2-propanol, and drying with N_2 gas.

Thin film samples of Irganox 1010 were prepared by spin coating as follows: 0.1 mL of solution was dropped onto a 1 cm^2 (1 cm × 1 cm) substrate (aluminum foil or silicon wafer) and the sample spun at 500 rpm for 10 s and then 2900 rpm for 12 s using a KW-4A spin-coater (Chemat Technology, Inc., Northridge, CA). This was repeated as many as five times. To investigate the effect of sample preparation on secondary ion yields, a second series of Irganox 1010 samples was prepared by allowing drops of solution to dry on the Al and Si substrates as follows:

Table 2. Negative ion secondary ion yields and yield enhancements for thin films of *DL*-phenylalanine adsorbed on silicon using 25 keV Bi_n^{2+} and Bi_n^+ primary ions

	Primary ion			
	Bi_3^{2+}	Bi_3^+	Bi^{2+}	Bi^+
Y([M – H]$^-$; *m/z* = 164)	5.5×10^{-4}	3.3×10^{-4}	1.6×10^{-4}	4.5×10^{-5}
$Y(Bi_n^{2+})/Y(Bi_n^+)$	1.7		3.6	

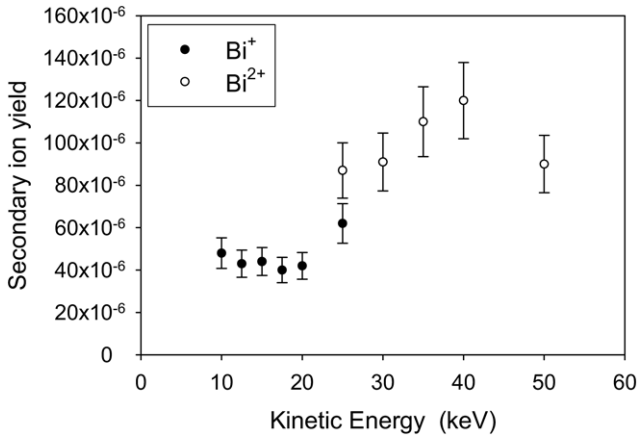

Figure 1. The variation of the secondary ion yields of the protonated molecular ion, $[M + H]^+$ (*m/z* 166) for *DL*-phenylalanine adsorbed on Si with primary ion incident kinetic energy for Bi_3^+ and Bi_3^{2+}.

0.1 mL was dropped onto a 1 cm^2 (1 cm × 1 cm) substrate (aluminum foil or silicon wafer) and allowed to dry. This was repeated as many as five times.

Samples of *DL*-phenylalanine were prepared by allowing one drop of solution (<0.1 mL) to evaporate on the substrate surface. Thick *DL*-phenylalanine samples were obtained from E. A. Schweikert, Texas A and M University, College Station, TX. The samples were prepared by vapor-deposition of *DL*-phenylalanine on silicon and the thickness is estimated to be 2500 Å using ellipsometry. Thin films of cholesterol, DPPC and DPPE were prepared by allowing one drop of solution (<0.1 mL) to evaporate on a Si substrate.

For the polymer films, 200 μL of solution was dropped onto a 1 cm^2 (1 cm × 1 cm) substrate (aluminum foil or silicon wafer) and the sample spun at 500 rpm for 10 s and then 2900 rpm for 12 s using a KW-4A spin-coater. This procedure was repeated five times.

Recent experiments using layered films demonstrate that although the vast majority of secondary ions are emitted from the top ~2 to 3 nm of a sample, some secondary ions from deep within samples are emitted (from depths ≥ 100 Å) [18]. Since we observe a few ions from the substrate in all SIMS spectra, except for the thick *DL*-phenylalanine samples, indicating that Bi_n^{x+} (n = 1, 3, 5; x = 1, 2) ions penetrate through the organic layer to the substrate, we estimate that the sample films are 50 to 300 Å thick.

Quantum Mechanical Calculations

Density functional theory (DFT) geometry optimization calculations were performed to determine the energy required to form the cation, $CH_2 = CHCH_2^+$, from the neutral species, $CH_2CH_2CH_2$. The calculations were carried out using the NWChem 4.5 program package [19, 20] at the PW91PW91/cc-pVDZ level of theory [21–25]. No thermal effects or zero-point energies are included.

DFT geometry optimization calculations were also performed to determine the lowest energy structures and ionization potentials for clusters with the formula Bi_n^+ and Bi_n (n = 1–5) at the PW91PW91/CRENBL level of theory [21, 26–31]. The accuracy of the computational method was checked by performing calculations on the Bi atom and Bi_2 cluster. Our calculated ionization potential (IP) for Bi_2 is 7.44 eV, which is in good agreement with experimental data [32]. However the calculated ionization potential and electron affinity of Bi are 8.03 eV and 0.69 eV, which are not in good agreement with experimental data (7.29 eV and 0.95 eV, respectively [33]. Further, the ionization potential of Bi_3 is 6.38 eV, which is much smaller than experimentally determined (IP = 8.8 ± 0.5 eV [34]. Furthermore, the binding energies of Bi_2 and Bi_2^+ are much larger, 5.1 eV and 5.7 eV, respectively, than the experimentally observed values of 2.06 eV [35] and 1.77 eV [36], respectively. These calculations were repeated PW91PW91/LANL2DZdp level of theory [21, 37–39], and nearly-identical lowest-energy structures and ionization and binding energies were found. Now it is not clear why the calculated energies differ from the experimental values.

Results and Discussion

Secondary Ion Yields: Phenylalanine, DPPC, DPPE, Cholesterol, and Irganox 1010

Table 1 displays secondary ion yields, Y, of the protonated molecular ion, $[M + H]^+$ (*m/z* 166) and a representative fragment ion, $C_8H_{10}N^+$ (*m/z* 120), for *DL*-phenylalanine

Table 3. Positive and negative ion secondary ion yields and yield enhancements for thick films of *L*-phenylalanine adsorbed on silicon using 25 keV Bi_n^{2+} and Bi_n^+ primary ions

Primary ion	$Y(C_8H_{10}N^+$; *m/z* 120)	$Y([M + H]^+$; *m/z* 166)	$Y([M - H]^-$; *m/z* 164)
Bi_3^+	1.1×10^{-3}	2.5×10^{-3}	2.4×10^{-3}
Bi_3^{2+}	5.0×10^{-3}	3.5×10^{-3}	8.9×10^{-3}
$Y(Bi_3^{2+})/Y(Bi_3^+)$	4.5	2.3	3.7
Bi^+	8.4×10^{-4}	1.0×10^{-3}	1.5×10^{-3}
Bi^{2+}	8.4×10^{-4}	9.3×10^{-3}	2.2×10^{-3}
$Y(Bi^{2+})/Y(Bi^+)$	1.0	9.0	1.5

Table 4. Positive ion secondary ion yields and yield enhancements for thin films of DPPC, DPPE, and cholesterol adsorbed on silicon using 25 keV Bi_n^{2+} and Bi_n^{+} primary ions

Fragment ions	*m/z*	$Y(Bi^{2+})$	$Y(Bi^{+})$	$Y(Bi^{2+})/Y(Bi^{+})$	$Y(Bi_3^{2+})$	$Y(Bi_3^{+})$	$Y(Bi_3^{2+})/Y(Bi_3^{+})$
DPPC							
$[C_5H_{15}\ N\ PO_4]^+$	184	4.8×10^{-4}	2.3×10^{-4}	2.0	6.9×10^{-3}	4.6×10^{-3}	1.5
$[C_{16}H_{32}]^+$	224	5.0×10^{-5}	2.2×10^{-5}	2.3	6.5×10^{-4}	5.2×10^{-4}	1.3
$[M + H]^+$	735	6.9×10^{-7}	1.9×10^{-7}	3.6	1.8×10^{-5}	1.5×10^{-5}	1.2
DPPE							
$[C_2H_7PO_3N]^+$	124	1.2×10^{-5}	7.4×10^{-6}	1.6	1.7×10^{-4}	6.4×10^{-5}	2.7
$[C_2H_9PO_4N]^+$	142	8.0×10^{-6}	4.4×10^{-6}	1.8	Not obs.	7.7×10^{-5}	-
$[C_{35}H_{57}O_4]^+$	552	5.4×10^{-6}	2.0×10^{-6}	2.7	1.4×10^{-4}	3.8×10^{-4}	2.7
Cholesterol							
$[M - OH]^+$	369	3.0×10^{-6}	1.5×10^{-6}	2.0	Not obs.	1.7×10^{-5}	-
$[M + H]^+$	385	7.2×10^{-6}	4.3×10^{-6}	1.7	9.1×10^{-5}	2.7×10^{-5}	3.4

adsorbed on Al and Si upon Bi_n^{+} and Bi_n^{2+} (n = 1, 3) primary ion bombardment at the same primary ion velocity. In contrast to previous experiments using Au [7] and Ar [15] primary ions, we observe that Bi^{2+} primary ion bombardment increases the secondary ion yield of the molecular ion by approximately three times compared with Bi^{+} primary ion bombardment for *DL*-phenylalanine films adsorbed on Si. Further, the secondary ion yields of the fragment ions are approximately twice as large for Bi^{2+} primary ions as for Bi^{+}. In the negative ion mass spectra, the secondary ion yields of the deprotonated molecular ion $[M - H]^-$ (*m/z* 164) are also larger using the doubly-charged primary ions (Table 2). Most of the molecular and fragment positive ion yields of *DL*-phenylalanine using Bi_n^{x+} (n = 1, 3; x = 1, 2) primary ions for DL-phenylalanine adsorbed on Al are the same within experimental error (±20%), in agreement with previous work [7, 15]. Now, it is not clear why the use of a silicon substrate causes an increase in the secondary ion yield when using Bi^{2+} and Bi_3^{2+} primary ions.

Figure 1 displays the variation of the secondary ion yields of the protonated molecular ion, $[M + H]^+$ (*m/z* 166) of *DL*-phenylalanine adsorbed on Si with primary ion incident kinetic energy. In contrast to previous studies [7], it can be seen that the trends in the secondary ion yields with incident primary kinetic energy are different for Bi^{2+} and Bi^{+}. For Bi^{2+}, the secondary ion yield increases with increasing kinetic energy and then appears to decrease at the highest incident kinetic energy, 50 keV. For Bi^{+} the secondary ion yield remains approximately constant until a kinetic energy of ~20 keV is reached and then increases. Similar data is obtained using Bi_3^{2+} and Bi_3^{+} primary ions (data not shown). There are two possible reasons for the observed difference in behavior for Bi and Au primary ion bombardment [7]. First, the thickness of the *DL*-phenylalanine target was different in the two experiments. To test whether the sample thickness plays a role in the observed secondary ion yield differences, the secondary ion yield of *DL*-phenylalanine was measured on a thick sample (thickness ~ 2500 Å). For Bi^{2+} and Bi_3^{2+} the secondary ion yields are larger for both the protonated molecular ion, $[M + H]^+$ (*m/z* 166), and the deprotonated molecular ion, $[M - H]^+$ (*m/z* 164) (Table 3). We also observe that for Bi_3^{2+} primary ion bombardment, the secondary ion yield of the fragment ion *m/z* 120 is 4.5 times larger than for Bi_3^{+}. A second reason may be that Bi is a more reactive species [40] and so different ion-molecule interactions may occur. Further experiments are required to confirm this hypothesis.

Differences in the secondary ion yields are also observed for thin films of DPPC, DPPE, and cholesterol (Table 4). Secondary ion yield enhancements between 1.3 and 3.4 are observed for doubly charged primary ion bombardment. We note that for the protonated molecular ion of DPPC ($[M + H]^+$ *m/z* 735) no secondary ion yield enhancement is observed for Bi_3^{2+} primary ions. The data also show that, in general, the secondary ion yield enhancements are larger for Bi^{2+} primary ions than for Bi_3^{2+}, suggesting that the number of constituent atoms in the primary ion affects the observed secondary ion yield enhancement. The data also indicate that the yield enhancements of the highest intensity fragment ions are different from those observed for the molecular ions. For example, for cholesterol using Bi_3^{2+} primary ions, the secondary ion yield enhancement is 3.4 for the protonated molecular ion ($[M - H]^+$ *m/z* 385) but the dehydrated molecular ion ($[M + H - H_2O]^+$ *m/z* 369) is not observed.

For Irganox 1010 films, differences in the molecular and fragment ion yields for both Bi_n^{2+} (n = 1, 3, 5) primary ions were also observed compared to Bi_n^{+} (Tables 5, 6, and 7). For Bi^{2+} ions, the secondary ion yields increase slightly both in the positive ion spectra (*m/z* 899) and in the negative ion spectra (*m/z* 1175; $[M - H]^-$) for Irganox 1010 adsorbed on Si (Table 5). Furthermore, in the positive ion spectra, the fragment ion at *m/z* 219 has a higher secondary ion yield enhancement (1.8) than the largest positive fragment ion, $[M + H - HOOC(CH_2)_2(C(CH)_2(C(CH_3)_3)_2(C(OH))]^{+\cdot}$, (*m/z* 899). This ion is drawn in Structure **2**

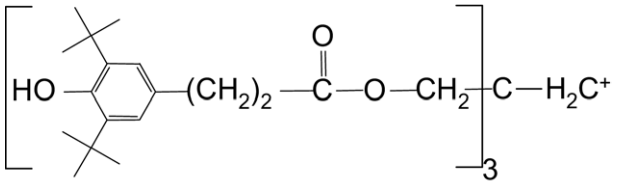

Structure 2. Structure of the largest positive fragment ion for Irganox 1010.

Table 5. Fragment and molecular ion yields and yield enhancements of Irganox 1010 adsorbed on silicon and aluminum substrates, using 25 keV Bi^{2+} and Bi^{+} primary ions

		Si			Al		
Fragment ions	*m/z*	$Y(Bi^{2+})$	$Y(Bi^{+})$	$Y(Bi^{2+})/Y(Bi^{+})$	$Y(Bi^{2+})$	$Y(Bi^{+})$	$Y(Bi^{2+})/Y(Bi^{+})$
Negative ions							
C_2HO^-	41	2.1×10^{-4}	1.0×10^{-4}	2.2	2.3×10^{-4}	1.7×10^{-4}	1.4
$C_{14}H_{21}O^-$	205	2.9×10^{-5}	1.5×10^{-5}	2.0	2.5×10^{-5}	1.8×10^{-5}	1.4
$C_{16}H_{23}O^-$	231	3.6×10^{-4}	1.7×10^{-4}	2.2	3.3×10^{-4}	2.3×10^{-5}	1.4
$C_{17}H_{25}O_3^-$	277	1.2×10^{-4}	5.4×10^{-5}	2.2	1.3×10^{-4}	9.0×10^{-5}	1.4
$C_{38}H_{55}O_6^-$	607	1.4×10^{-6}	7.2×10^{-7}	1.9	1.4×10^{-6}	1.5×10^{-6}	0.9
$C_{56}H_{83}O_{10}^-$	915	1.2×10^{-6}	1.1×10^{-6}	1.1	2.6×10^{-6}	2.9×10^{-6}	0.9
$C_{73}H_{17}O_{12}^-$	1175	2.8×10^{-5}	1.4×10^{-5}	2.0	3.6×10^{-5}	3.0×10^{-5}	1.2
Positive Ions							
$C_4H_9^+$	57	4.2×10^{-3}	3.3×10^{-3}	1.3	4.3×10^{-3}	3.5×10^{-3}	1.2
$C_7H_7^+$	91	3.0×10^{-4}	2.3×10^{-4}	1.3	3.1×10^{-4}	3.0×10^{-4}	1.0
$C_{15}H_{23}O^+$	219	8.4×10^{-3}	4.6×10^{-3}	1.8	7.7×10^{-3}	4.8×10^{-3}	1.6
$C_{17}H_{23}O_2^+$	259	1.0×10^{-3}	8.8×10^{-4}	1.1	9.7×10^{-4}	1.1×10^{-3}	0.9
$C_{31}H_{43}O_7^+$	527	2.8×10^{-5}	2.0×10^{-5}	1.4	2.5×10^{-5}	2.3×10^{-5}	1.1
$C_{35}H_{51}O_7^+$	583	1.2×10^{-5}	1.0×10^{-5}	1.2	1.3×10^{-5}	1.3×10^{-5}	1.0
$C_{44}H_{59}O_9^+$	731	4.3×10^{-5}	3.2×10^{-5}	1.3	3.5×10^{-5}	3.5×10^{-5}	1.0
$C_{56}H_{83}O_9^+$	899	4.9×10^{-5}	3.3×10^{-5}	1.5	4.4×10^{-5}	4.5×10^{-5}	1.0

and will be hereafter denoted as A^+. In the negative ion spectra the fragment ions have secondary ion yield enhancements similar to those observed for the molecular ion. For Irganox 1010 adsorbed on Al, for Bi^{2+} primary ion bombardment we observe that most of the molecular and fragment ion yields are the same within experimental error (±20%). However, there are some exceptions: in the positive ion mass spectrum, the secondary ion yield of the fragment ion at *m/z* 219 is enhanced by ~60%. In the negative ion mass spectra, the secondary ion yields of the fragment ions with *m/z* below 300 are slightly larger. All these ions derive from the Irganox 1010 monomer and suggest that using Bi^{2+} primary ions increase the fragmentation of Irganox 1010.

For Bi_3^{2+} primary ions, in the negative ion mode the deprotonated molecular ion yield (*m/z* 1175; $[-H]^-$) is larger than for Bi_3^+ primary ions for Irganox 1010 adsorbed on both Al and Si substrates (Table 6). However, the observed fragment ion behavior is different for Irganox 1010 adsorbed on Si and Al substrates. For Irganox 1010 adsorbed on Al, the secondary ion yields for the fragment ions are the same for Bi_3^{2+} and Bi_3^+ primary ions within experimental error (±20%). For Irganox 1010 adsorbed on Si, the secondary ion yields of the fragment ions at *m/z* 41, 231, 277, and 915 are enhanced for Bi_3^{2+} primary ions. Further, the secondary ion yield enhancements of the fragment ions at *m/z* 41 and *m/z* 231 are larger than for the deprotonated molecular

Table 6. Fragment and molecular ion yields and yield enhancements of Irganox 1010 adsorbed on silicon and aluminum substrates, using 25 keV Bi_3^{2+} and Bi_3^+ primary ions

		Si			Al		
Fragment ions	*m/z*	$Y(Bi_3^{2+})$	$Y(Bi_3^+)$	$Y(Bi_3^{2+})/Y(Bi_3^+)$	$Y(Bi_3^{2+})$	$Y(Bi_3^+)$	$Y(Bi_3^{2+})/Y(Bi_3^+)$
Negative ions							
C_2HO^-	41	3.8×10^{-3}	2.1×10^{-3}	1.8	2.8×10^{-3}	3.4×10^{-3}	0.8
$C_{14}H_{21}O^-$	205	3.3×10^{-4}	2.8×10^{-4}	1.2	2.1×10^{-4}	2.5×10^{-4}	0.8
$C_{16}H_{23}O^-$	231	3.3×10^{-3}	1.9×10^{-3}	1.8	2.0×10^{-4}	2.3×10^{-4}	0.9
$C_{17}H_{25}O_3^-$	277	8.9×10^{-4}	6.9×10^{-4}	1.3	5.8×10^{-4}	7.5×10^{-4}	0.8
$C_{38}H_{55}O_6^-$	607	9.3×10^{-6}	7.8×10^{-6}	1.2	1.1×10^{-5}	9.3×10^{-6}	1.2
$C_{56}H_{83}O_{10}^-$	915	3.6×10^{-5}	2.6×10^{-5}	1.4	3.0×10^{-5}	2.8×10^{-5}	1.1
$C_{73}H_{17}O_{12}^-$	1175	5.4×10^{-4}	3.6×10^{-4}	1.5	5.3×10^{-4}	3.8×10^{-4}	1.4
Positive ions							
$C_4H_9^+$	57	3.7×10^{-2}	1.4×10^{-2}	2.6	2.1×10^{-2}	2.0×10^{-2}	1.1
$C_7H_7^+$	91	3.5×10^{-3}	3.3×10^{-3}	1.1	2.3×10^{-3}	2.5×10^{-3}	0.9
$C_{15}H_{23}O^+$	219	5.8×10^{-2}	7.7×10^{-3}	7.5	3.0×10^{-2}	1.7×10^{-2}	1.8
$C_{17}H_{23}O_2^+$	259	6.9×10^{-3}	9.0×10^{-3}	0.8	3.8×10^{-3}	7.6×10^{-3}	0.5
$C_{31}H_{43}O_7^+$	527	2.4×10^{-4}	2.8×10^{-4}	0.9	8.3×10^{-5}	1.8×10^{-4}	0.5
$C_{35}H_{51}O_7^+$	583	1.2×10^{-4}	1.4×10^{-4}	0.9	4.5×10^{-5}	9.5×10^{-5}	0.5
$C_{44}H_{59}O_9^+$	731	3.6×10^{-4}	4.9×10^{-4}	0.7	1.7×10^{-4}	3.5×10^{-4}	0.5
$C_{56}H_{83}O_9^+$	899	5.1×10^{-4}	6.3×10^{-4}	0.8	2.7×10^{-4}	4.8×10^{-4}	0.6

Table 7. Fragment and molecular ion yields and yield enhancements of Irganox 1010 adsorbed on silicon and aluminum substrates, using 25 keV Bi_5^{2+} and Bi_5^{+} primary ions

		Si			Al		
Fragment ions	*m/z*	$Y(Bi_5^{2+})$	$Y(Bi_5^{+})$	$Y(Bi_5^{2+})/Y(Bi_5^{+})$	$Y(Bi_5^{2+})$	$Y(Bi_5^{+})$	$Y(Bi_5^{2+})/Y(Bi_5^{+})$
Negative ions							
C_2HO^-	41	2.6×10^{-3}	2.9×10^{-3}	0.9	1.6×10^{-3}	1.6×10^{-3}	1.0
$C_{14}H_{21}O^-$	205	1.9×10^{-4}	2.0×10^{-4}	1.0	1.5×10^{-4}	9.6×10^{-5}	1.6
$C_{16}H_{23}O^-$	231	1.9×10^{-3}	1.8×10^{-3}	1.0	8.9×10^{-4}	9.0×10^{-4}	1.0
$C_{17}H_{25}O_3^-$	277	4.6×10^{-4}	5.5×10^{-4}	0.8	2.5×10^{-4}	1.8×10^{-4}	1.4
$C_{38}H_{55}O_6^-$	607	4.5×10^{-6}	4.9×10^{-6}	0.9	2.5×10^{-6}	2.0×10^{-6}	1.3
$C_{56}H_{83}O_{10}^-$	915	1.6×10^{-5}	2.0×10^{-5}	0.8	1.1×10^{-5}	1.1×10^{-5}	1.0
$C_{73}H_{17}O_{12}^-$	1175	2.9×10^{-4}	3.0×10^{-4}	1.0	2.8×10^{-4}	2.0×10^{-4}	1.5
Positive ions							
$C_4H_9^+$	57	1.3×10^{-2}	6.7×10^{-2}	0.19	7.5×10^{-3}	4.0×10^{-2}	0.19
$C_7H_7^+$	91	3.2×10^{-3}	1.2×10^{-2}	0.26	2.0×10^{-3}	7.3×10^{-2}	0.27
$C_{15}H_{23}O^+$	219	1.8×10^{-2}	8.2×10^{-2}	0.21	7.6×10^{-3}	4.1×10^{-2}	0.19
$C_{17}H_{23}O_2^+$	259	1.9×10^{-3}	1.1×10^{-2}	0.17	6.8×10^{-4}	4.2×10^{-3}	0.16
$C_{31}H_{43}O_7^+$	527	5.0×10^{-5}	2.5×10^{-4}	0.20	2.7×10^{-5}	1.6×10^{-4}	0.16
$C_{35}H_{51}O_7^+$	583	2.0×10^{-5}	1.2×10^{-4}	0.17	1.4×10^{-5}	8.2×10^{-4}	0.17
$C_{44}H_{59}O_9^+$	731	7.8×10^{-5}	5.2×10^{-4}	0.15	5.3×10^{-5}	3.2×10^{-4}	0.17
$C_{56}H_{83}O_9^+$	899	1.1×10^{-4}	5.1×10^{-4}	0.21	6.4×10^{-5}	3.6×10^{-4}	0.17

ion, $[M - H]^-$ (*m/z* 1175). In general, for Bi_3^{2+} in the positive ion mass spectra the secondary ion yields of the fragment ions are the same (Irganox 1010 adsorbed on Si) or lower (Irganox 1010 adsorbed on Al) than for Bi_3^{+}. However for both Irganox 1010 adsorbed on Si and Al the secondary ion yield for the fragment ion at *m/z* 219 is larger for Bi_3^{2+} primary ion bombardment.

Liquid metal bismuth ion sources are also able to produce Bi_5^{+} and Bi_5^{2+} ions with low ion currents. In the negative ion mass spectra the secondary ion yields are approximately the same for Bi_5^{2+} and Bi_5^{+} for Irganox 1010 adsorbed on Si (Table 7). For Irganox 1010 adsorbed on Al in the negative ion mode the secondary ion yields are the same or slightly larger for the doubly-charged ions. However, in the positive ion mass spectrum the secondary ion yields for Bi_5^{2+} are only ~20% of those observed for Bi_5^{+}.

The secondary ion yields for Bi_3^{x+} and Bi_5^{x+} are larger than for Bi^{x+} (x = 1, 2) in agreement with previous studies which show that the secondary ion yields increase with increasing number of primary ion constituent atoms [6, 7, 9, 11, 13]. However, the secondary ion yields for Bi_3^{x+} primary ion bombardment are in general larger than for Bi_5^{x+}. This is most likely due to the decrease in projectile velocity balancing the expected increase in the secondary ion yield attributable to the increase in the number of projectile constituent atoms (see [6, 13] and references therein). We note that the secondary yield enhancements due to the doubly charged ions decrease with increasing primary ion constituent number; the yield enhancements are larger for Bi^{2+} than Bi_3^{2+}, which in turn are larger than for Bi_5^{2+} primary ions. This suggests that the number of constituent atoms in the primary ion has a larger effect on the secondary ion yield than changing the primary ion charge from +1 to +2.

We also note that the magnitude of the secondary ion yield enhancement, or lack of it, depends on the sample preparation. For example, for samples prepared by allowing one drop of a 1 mg/mL Irganox 1010 solution to dry on a Si or Al substrate, secondary ion yield enhancements for the deprotonated molecular ion, $[M - H]^-$ (*m/z* 1175), vary from 0.9 to 4.7, as shown in Figure 2. However, if the samples are spun-coat, the observed secondary ion yield enhancements are very similar from sample to sample with slightly larger secondary ion yield enhancements observed for multiple coating steps (Figure 2). In general, the relative ion

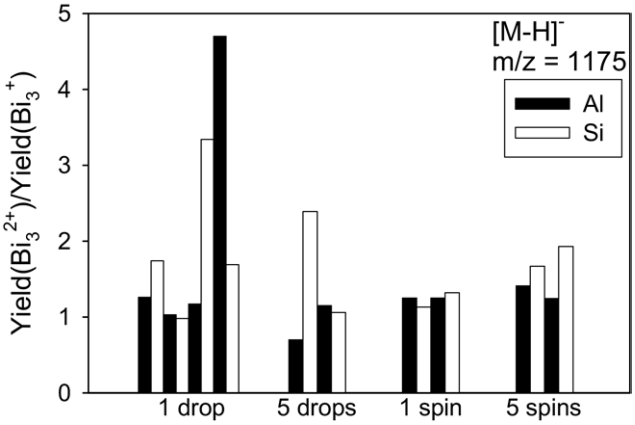

Figure 2. Secondary ion yield enhancements of the deprotonated molecular ion, $[M - H]^-$ (*m/z* 1175), using Bi_3^{2+} primary ions for Irganox 1010 adsorbed on Al and Si substrates under different sample preparation conditions: a single drop of solution dried on the substrate ("1 drop"), repeating this procedure a five times ("5 drops"), spin-coating the sample after placing 1 drop of solution on the sample ("1 spin") and repeating the spin-coating procedure 5 times ("5 spins"). Each bar represents a single sample. The secondary ion yields and yield enhancements were determined for three points on the sample and then averaged.

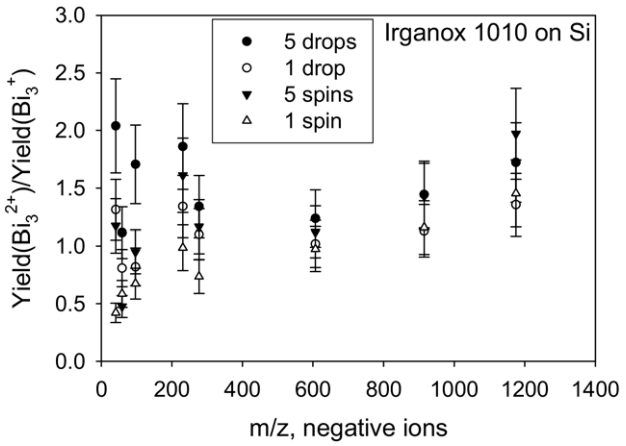

Figure 3. Yield ratios ($Y[Bi_3^{2+}]/Y[Bi_3^{+}]$) at a constant primary ion incident kinetic energy (25 keV) versus *m/z* for Irganox 1010 adsorbed on Si under different sample conditions: a single drop of solution dried on the substrate ("1 drop"), repeating this procedure a five times ("5 drops"), spin-coating the sample after placing 1 drop of solution on the sample ("1 spin"), and repeating the spin-coating procedure five times ("5 spins"). Each data symbol represents a single sample. The secondary ion yields and yield enhancements were determined for three points on the sample and then averaged.

yields of the fragment ions do not appear to be affected by the sample preparation method (Figure 3). The yield enhancements observed for the fragment ions follow the same trends: the secondary ion yield and yield enhancements decrease to a minimum at *m/z* ~ 500 and then increase to the deprotonated molecular ion, $[M - H]^-$ (*m/z* 1175). We note that this behavior is similar to that observed for Irganox 1010 films bombarded with Au_n^+ [13] and Bi_n^+ (n = 1–7) [6] primary ions. Spin-coating is known to produce samples of more uniform, reproducible thickness, and so the most likely reason for the observed differences in the yield enhancements for the drop-coat samples (Figure 2) is that the Irganox 1010 film has a different thickness on each substrate.

A second possible factor that could affect the secondary ion yield enhancements is the substrate. For Au_n^+ [13] and Bi_n^+ [6] (n = 1–7) secondary ion yield enhancements are generally larger on Si (atomic weight 28.086; diamond structure; density 2.33 g cm^{-3} [33] than on Al (atomic weight: 26.982; face-centered cubic structure; density 2.70 g cm^{-3} [33]. For *DL*-phenylalanine and Irganox 1010, the yield enhancements observed for doubly charged primary ions are in general slightly larger on Si than on Al, suggesting that there is more efficient energy transfer on the more open Si substrate. However, further investigation is required to determine the magnitude of this effect.

The fragment and molecular secondary ion yields from *DL*-phenylalanine and Irganox 1010 exhibit different behavior for Bi_n^{2+} primary ions compared with Bi_n^+ ion bombardment. It seems unlikely that the differences observed are due to changes in the sputtering rate of the doubly charged Bi primary ions, since the primary ions strike the surface at the same impact velocity. Further, the observed secondary ion yield enhancements (or lack thereof) differ in the negative and positive ion mass spectra, and they are dependent on the sample preparation employed. Taken together, these data suggest that the ionization mechanism is different for doubly charged and singly charged primary ions.

Secondary Ion Yields: Polymer Films

To further investigate yield enhancements in Bi^{2+}, Bi_3^{2+}, and Bi_5^{2+} SIMS, polymer films were spun-coat onto clean silicon substrates to have a series of sample films with similar thicknesses but different chemistries. The polymers chosen were PE, PI, PS, PEO, PPG, PEG, PDMPO, and PMMA, and their structures are shown in Structure **1**.

For all the polymer films investigated upon Bi_n^{2+} (n = 1, 3, 5) primary ion bombardment the intensities of the secondary ions from the oligomer regions were greatly reduced or eliminated using Bi_n^{2+} primary ions. For example, in Figures 4a and 5a we show for PS and PE, respectively, that no ions are observed above *m/z* ~ 400. For PDMPO films, a few ions above *m/z* ~ 400 are observed (Figure 6a). In contrast, secondary ions from the oligomer regions are observed in the mass spectra for Bi_n^+ (n = 1, 3, 5) primary ion bombardment (see for example Figures 4b, 5b, and 6b).

For PS, PEO, PEG, and PPG the intensities of fragment ions indicative of the monomer are enhanced when using Bi^{2+} and Bi_3^{2+} ions (Figure 4c, d and Figure 5c, d; Table 8). Secondary ion yield enhancements observed range from 1.3 to 4.3. For PS there are three monomer ions observed, with only the tropylium ion, $C_7H_7^+$ (*m/z* 91) exhibiting a secondary ion yield enhancement. For Bi_3^{2+} primary ion bombardment of PI, the secondary ion yields at *m/z* 69 and 81 were approximately the same as for Bi_3^+ primary ions at the same velocity. For PDMPO and PMMA, no secondary ion yield enhancement was observed for doubly charged ion bombardment. For Bi^{2+} and Bi_3^{2+} primary ion bombardment the secondary ion yields of monomer ions were observed to decrease to ~60% and ~20% of their values when using singly charged primary ions for PMMA and PDMPO, respectively (Table 8). In contrast to Bi^{2+} and Bi_3^{2+}, no secondary ion yield enhancements are observed using Bi_5^{2+} primary ions; for all polymers studied the monomer ion yields are ~25% of their values when using Bi_5^+. In agreement with our studies on Irganox 1010, these observations suggest that the atomicity of the primary ion has a larger effect on the secondary ion yields than changing the primary ion charge from +1 to +2. These measurements also suggest that use of multiply charged primary ions can lead to the suppression of secondary ion formation. To our knowledge, this is the first time in SIMS that secondary ion suppression has been induced by changing the charge state of the primary ion. Secondary ion suppression is well known in fast atom bombardment (FAB)

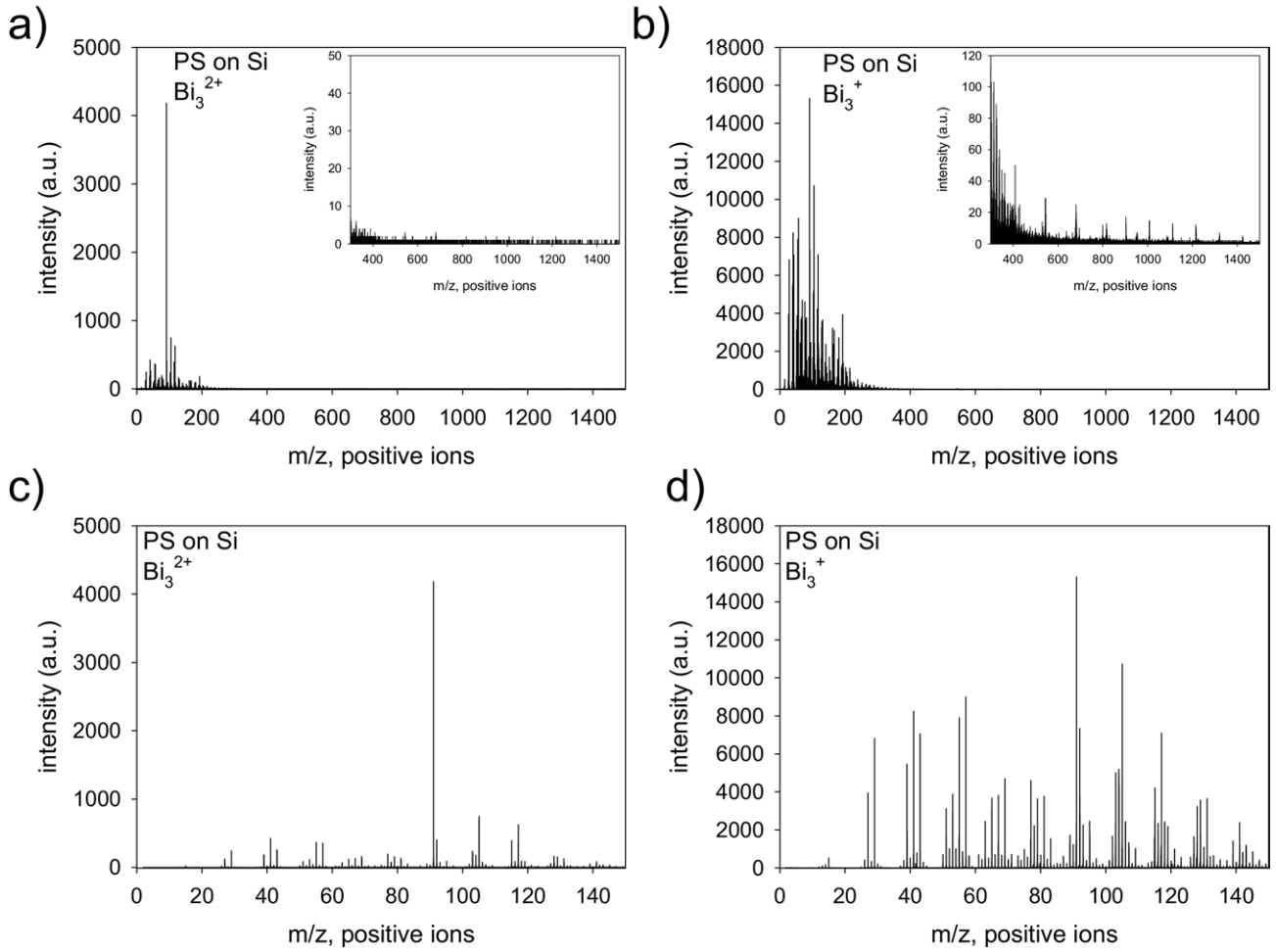

Figure 4. TOF SIMS positive ion mass spectra of PS adsorbed on Si under (**a**) Bi_3^{2+} and (**b**) Bi_3^+ primary ion bombardment for *m/z* 0—1500. The insets are the mass spectra in the range *m/z* = 300–1500. Mass spectra of the monomer region (*m/z* 0–150) are shown under (**c**) Bi_3^{2+} and (**d**) Bi_3^+ primary ion bombardment.

and is due matrix effects [41]. However, it is not clear why suppression of certain secondary ions is occurring in these experiments. Further work is required to determine the origin of this effect.

The common feature of the polymers that display increased secondary ion yields is that the polymer backbone contains -CH_2-CH_2- structures. These polymers can undergo allyl radical cation rearrangement (Scheme **1**).In contrast, PDMPO and PMMA cannot undergo allyl radical cation rearrangements. Thus one possible reason for the observed larger secondary ion yields for PE, PEO, PEG and PPG is that the monomer ions undergo allyl cation radical rearrangements. Since the doubly and singly charged primary ions have the same impact energy, these observations suggest the extra energy available from the second ionization potential (IP) of the Bi_n (n = 1, 3) primary ions activates this process. To investigate this possibility, we performed DFT calculations at the PW91PW91/cc-pVDZ level of theory to determine the energy required to form the cation:

$$CH_2CH_2CH_2 \rightarrow CH_2 = \overset{+}{C}HCH_2 + H + e^- \quad \Delta E(\text{calculated}) = 17.2 \text{ eV}$$

Calculations were performed using the NWChem 4.5 package [20], and both product and reactant molecules were geometry-optimized. No thermal effects or zero-point energies were included.

The reaction energy is larger than the ionization potential of Bi (IP = 7.29 eV [33] and Bi_3 (IP = 8.8 ± 0.5 eV [33]. However, the calculated ΔE is similar to the experimentally determined second ionization potential of Bi (IP = 16.69 eV [33], so the allyl radical cation rearrangement can be "powered" by reduction of Bi^{2+}. In the case of PS, the rearrangement causes the formation of the tropylium ion, $C_7H_7^+$ (*m/z* 91). The enthalpy of formation of the tropylium ion is 9 eV, which is similar to the first ionization potential of Bi_n [42]. Thus, the tropylium ion can also form upon Bi_n^+ primary ion bombardment. However, the extra

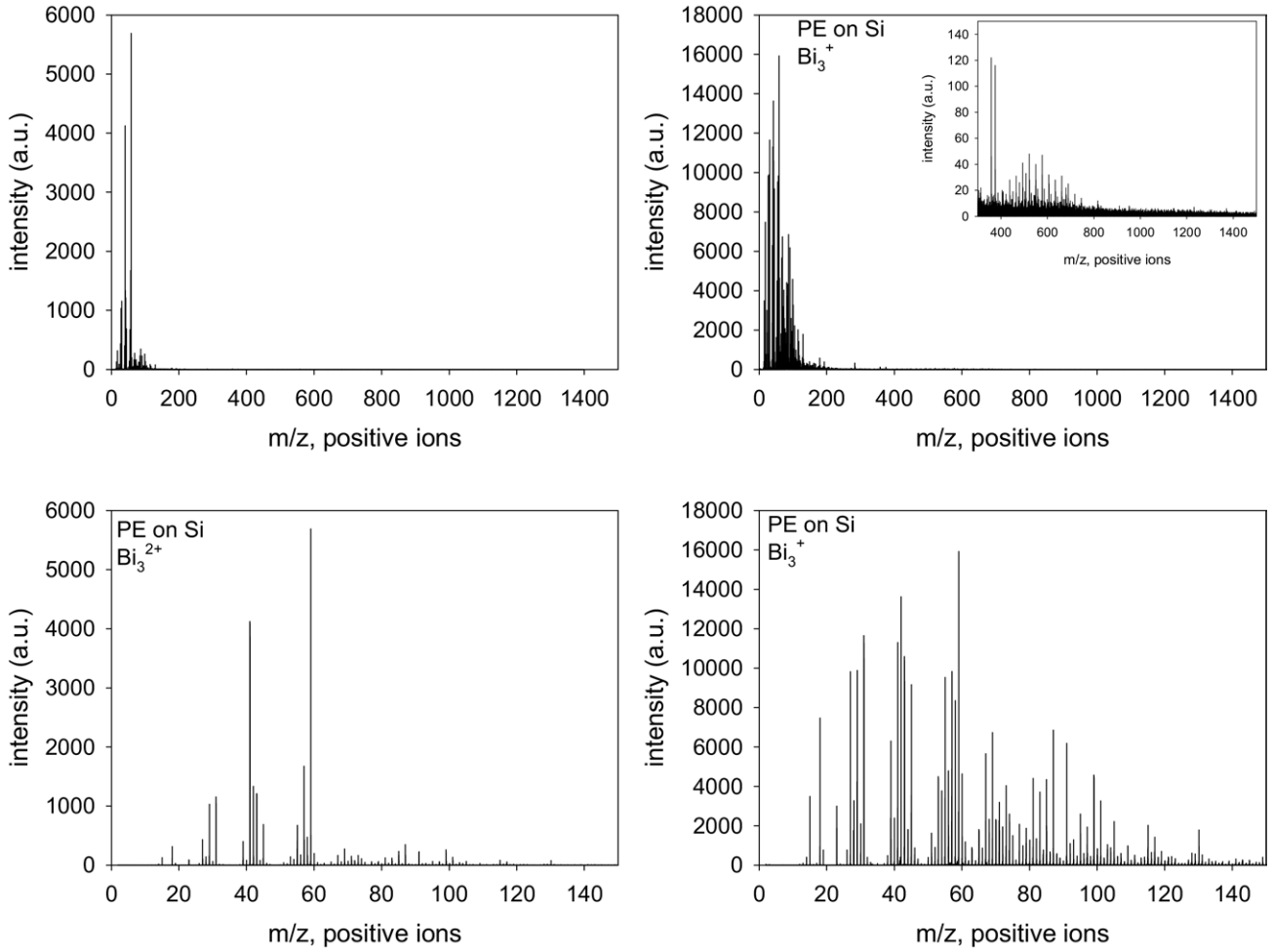

Figure 5. TOF SIMS positive ion mass spectra of PE adsorbed on Si under (**a**) Bi_3^{2+} and (**b**) Bi_3^+ primary ion bombardment for *m/z* 0–1500. The insets are the mass spectra in the range *m/z* = 300–1500. Mass spectra of the monomer region (*m/z* = 0–150) are shown under (**c**) Bi_3^{2+} and (**d**) Bi_3^+ primary ion bombardment.

energy from the second ionization potential will still favor the formation of these ions. Similar effects have been observed in the mass spectrometry of aromatic hydrocarbons; at 15 eV ionization energy the ratio of the benzyl ion to the tropylium ion is ~1:1 but if the ionization energy is increased to 70 eV the ratio of the tropylium ion to benzyl ion increases to 2:1 [42]. To our knowledge there is no experimentally reported value for the ionization potential of Bi_3^+ (that is, the second ionization potential of Bi_3). Attempts to calculate the Bi_3^+ ionization potential using standard methods did not give reliable results. However, it seems likely that the ionization potential of Bi_3^+ will also be high enough to promote the allyl radical cation rearrangement of PS, PEO, PEG, PPG, and PE. Finally we note that the PI backbone already contains a structure that could arise from this rearrangement, $-CH_2-C(CH_3)=CH-$. Thus, it is unlikely that the extra energy provided by the Bi_n^{2+} (n = 1, 3) primary ions will greatly increase the number of allyl radical cations formed, in agreement with our experimental observations of no secondary ion yield enhancement in the material.

Conclusions

We have investigated secondary ion yield enhancements using Bi^{2+}, Bi_3^{2+} and Bi_5^{2+} primary ions and phenylalanine, DPPC, DPPE, cholesterol, Irganox 1010 and polymer thin films adsorbed on silicon and aluminum. Secondary ion yield enhancements (or lack thereof) are dependent on the chemical nature of the sample and its preparation. The yield enhancements are different in the positive and negative mass spectra and vary between the fragment and molecular ions. The yield enhancements also decrease with increasing projectile atomicity, indicating that the number of projectile constituent atoms has a larger effect on the secondary ion yields. These observations indicate that the ionization mechanism is different for Bi_n^{2+} and Bi_n^+ (n = 1,3,5) primary ion bombardments. For Bi_n^{2+} (n = 1,3) the intensities of the

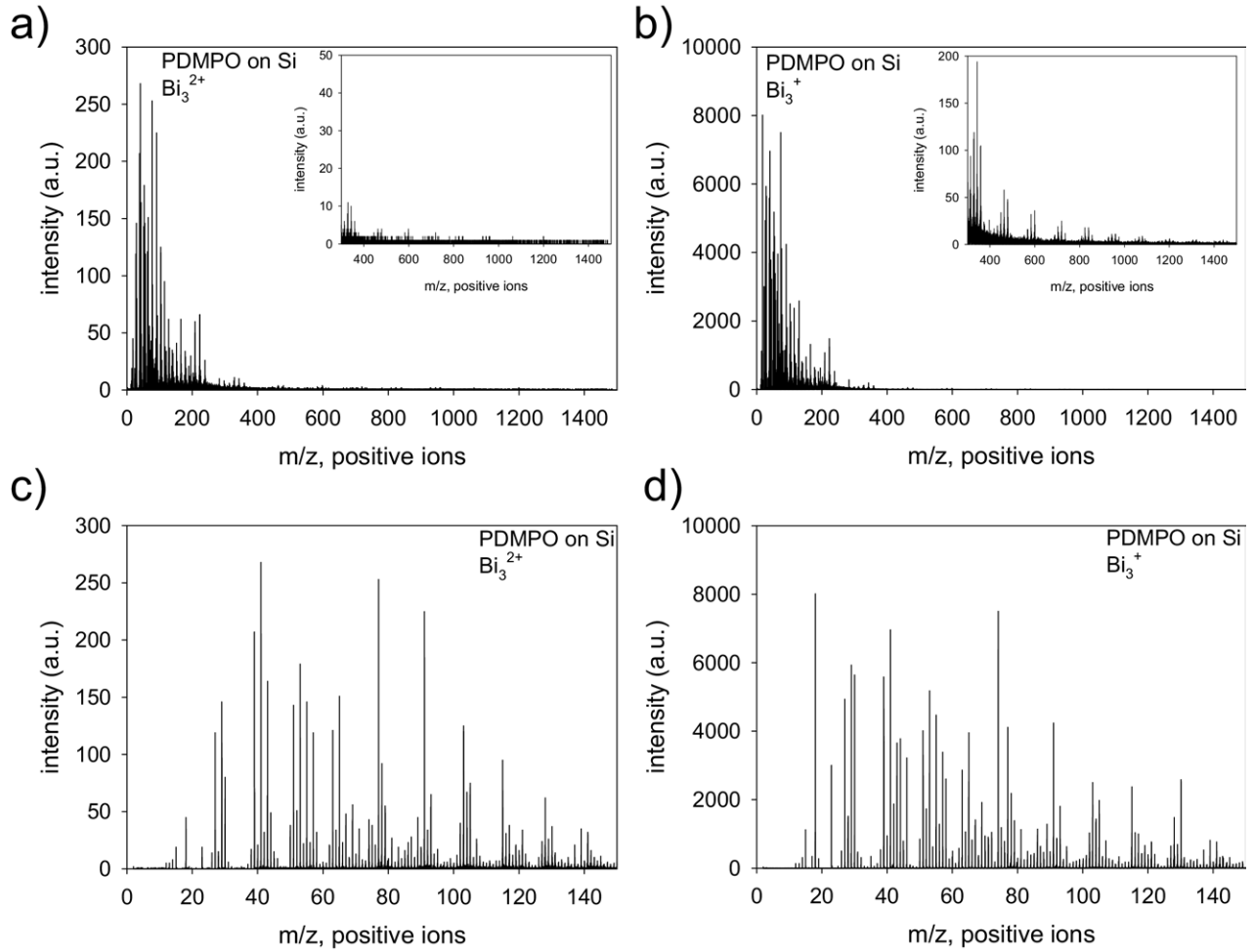

Figure 6. TOF SIMS positive ion mass spectra of PDMPO adsorbed on Si under (**a**) Bi_3^{2+} and (**b**) Bi_3^{+} primary ion bombardment for *m/z* 0–1500. The insets are the mass spectra in the range *m/z* 300–1500. Mass spectra of the monomer region (*m/z* 0–150) are shown under (**c**) Bi_3^{2+} and (**d**) Bi_3^{+} primary ion bombardment.

monomer ions are increased for polymers that are able to undergo allyl radical cation rearrangements. Observed secondary ion yield enhancements range from 1.2 to 4. Doubly-charged primary ions can also suppress secondary ion formation. For polymers that cannot undergo allyl cation rearrangements, the sec-

Table 8. Monomer ion yield enhancements observed from polymers adsorbed on silicon substrates, using 25 keV Bi_n^{2+} and Bi_n^{+} (n = 1, 3) primary ions

Polymer	Fragment	*m/zy*	$Y(Bi_3^{2+})$	$Y(Bi_3^{+})$	$Y(Bi_3^{2+})/Y(Bi_3^{+})$
PS	$C_7H_7^+$	91	5.0×10^{-3}	2.3×10^{-3}	2.2
	$C_8H_8^+$	104	7.9×10^{-4}	1.0×10^{-3}	0.8
	$C_9H_{10}^+$	118	3.6×10^{-4}	1.1×10^{-3}	0.3
PE	$C_2H_5^+$	29	1.0×10^{-3}	1.9×10^{-3}	0.5
	$C_3H_5^+$	41	3.7×10^{-3}	1.9×10^{-3}	1.9
PI	$C_5H_9^+$	69	1.8×10^{-3}	1.7×10^{-3}	1.0
	$C_6H_9^+$	81	2.0×10^{-3}	1.9×10^{-3}	1.1
PEO	$C_2H_4O^+$	45	2.0×10^{-3}	1.5×10^{-3}	1.3
PPG	$C_3H_5O^+$	59	1.1×10^{-2}	2.6×10^{-2}	4.3
PEG	$C_2H_4O^+$	45	8.6×10^{-3}	3.2×10^{-3}	2.7
PMMA	$C_5O_2H_9^+$	101	2.3×10^{-4}	1.1×10^{-3}	0.6
PDMPO	$C_6H_5^+$	77	2.3×10^{-4}	1.1×10^{-3}	0.2
	$C_7H_7^+$	91	2.5×10^{-4}	1.3×10^{-3}	0.2
	$C_8H_9O^+$	121	4.9×10^{-5}	3.5×10^{-5}	0.2

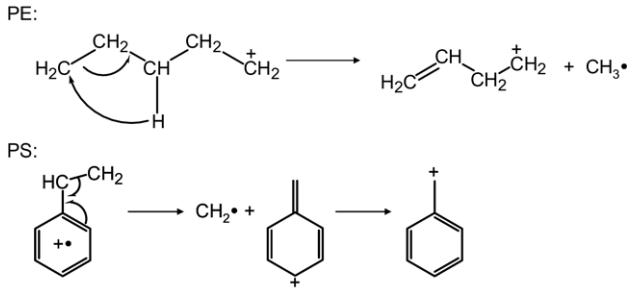

Scheme 1. Allyl radical cation rearrangements of PE and PS [19].

ondary ion yields of the monomer ions using Bi_n^{2+} (n = 1,3) primary ions are lower than for Bi_n^{+} primary ion bombardment. No secondary ion yield enhancements are observed using Bi_5^{2+} primary ions: for all polymers studied the monomer ion yields are ~25% of their values when using Bi_5^{+}. This behavior is not yet understood and further experiments are needed to investigate this effect. Finally, for all polymers studied, few or no secondary ions are observed in the oligomer region using Bi_n^{2+} (n = 1,3,5) primary ions. Taken together, these data indicate that primary ions of varying charge can be employed to enhance and also suppress ion intensities. This suggests that improvements in the analysis of complex chemical systems in SIMS may be made by judicious choice of primary ion beam.

Acknowledgments

The authors acknowledge the financial support of the National Science Foundation (CHE-0518063). The authors thank Z. Li and E. A. Schweikert for supplying thick vapor-deposited phenylalanine samples. AVW thanks M. L. Gross for many useful discussions. This work made use of the Washington University Computational Chemistry Facility, supported by NSF grant CHE-0443501.

References

1. *TOF SIMS: Surface Analysis by Mass Spectrometry*; Vickerman, J. C., Briggs, D., Eds.; IM Publications and Surface Spectra Ltd.: 2001.
2. Walker, A. V. Secondary Ion Mass Spectrometry and Fast Atom Bombardment: Principles and Instrumentation. In *The Encyclopedia of Mass Spectrometry*, Vol. VI; Gross, M. L.; Caprioli, R. M., Eds.; Elsevier: Oxford, UK, 2007; pp. 535–551.
3. Winograd, N. The Magic of Cluster SIMS. *Anal. Chem.* **2005,** *77,* 143A–149A.
4. Kollmer, F. Cluster Primary Ion Bombardment of Organic Materials. *Appl. Surf. Sci.* **2004,** *231/232,* 153–158.
5. Touboul, D.; Kollmer, F.; Niehuis, E.; Brunelle, A.; Laprévote, O. Improvement of Biological Time-of-Flight Secondary Ion Mass Spectrometry with a Bismuth Cluster Ion Source. *J. Am. Soc. Mass Spectrom.* **2005,** *16,* 1608–1618.
6. Nagy, G.; Walker, A. V. Enhanced Secondary Ion Emission with a Bismuth Cluster Ion Source. *Int. J. Mass Spectrom.* **2007,** *262,* 144–153.
7. Benguerba, M.; Brunelle, A.; Della-Negra, S.; Depauw, J.; Joret, H.; Le Beyec, Y.; Blain, M. G.; Schweikert, E. A.; Ben Assayag, G.; Sudrand, P. Impact of Slow Gold Clusters on Various Solids: Nonlinear Effects in Secondary Ion Emission. *Nucl. Instrum. Methods Phys. Res. B* **1991,** *62,* 8–22.
8. Walker, A. V.; Winograd, N. Prospects for Imaging with TOF-SIMS Using Gold Liquid Metal Ion Sources. *Appl. Surf. Sci.* **2003,** *203/204,* 198–200.
9. Boussofiane-Baudin, K.; Bolbach, G.; Brunelle, A.; Della-Negra, S.; Håkanson, P.; Le Beyec, Y. Secondary Ion Emission Under Cluster Impact at Low Energies (5–60 keV) Influence of the Number of Atoms in the Projectile. *Nucl. Instrum. Methods Phys. Res. B* **1994,** *88,* 160–163.
10. Boussofiane-Baudin, K.; Brunelle, A.; Chaurand, P.; Della-Negra, S.; Depauw, J.; Håkanson, P.; Le Beyec, Y. Nonlinear Sputtering Effects Induced by MeV Energy Gold Clusters. *Nucl. Instrum. Methods Phys. Res. B* **1994,** *88,* 61–68.
11. Brunelle, A.; Della-Negra, S.; Depauw, J.; Jacquet, D.; Le Beyec, Y.; Pautrat, M.; Baudin, K.; Andersen, H. H. Enhanced Secondary-Ion Emission Under Gold-Cluster Bombardment with Energies from keV to MeV per Atom. *Phys. Rev. A* **2001,** *63,* 022902/01–022902/10.
12. Davies, N.; Weibel, D. E.; Blenkinsopp, P.; Lockyer, N. P.; Hill, R.; Vickerman, J. C. Development and Experimental Application of a Gold Liquid Metal Ion Source. *Appl. Surf. Sci.* **2003,** *203/204,* 223–227.
13. Nagy, G.; Gelb, L. D.; Walker, A. V. An Investigation of Enhanced Secondary Ion Emission under Au_n^+ (n = 1–7) Bombardment. *J. Am. Soc. Mass Spectrom.* **2005,** *16,* 733–745.
14. Aumayr, F.; Winter, H. Potential Sputtering. *Philos. Trans. R. Soc. London A* **2004,** *362,* 77–102.
15. Della-Negra, S.; Depauw, J.; Joret, H.; Le Beyec, Y.; Schweikert, E. A. Secondary Ion Emission Induced by Multicharged 18-keV Ion Bombardment of Solid Targets. *Phys. Rev. Lett.* **1988,** *60,* 948–951.
16. Kakutani, N.; Azuma, T.; Yamazaki, Y.; Komaki, K.; Kuroki, K. Strong Charge State Dependence of H^+ and H_2^+ Sputtering Induced by Slow Highly Charged Ions *Nucl. Instrum. Methods Phys. Res. B* **1995,** *96,* 541–544.
17. Stephan, T.; Zehnpfenning, J.; Benninghoven, A. Correction of Dead Time Effects in Time-of-flight Mass Spectrometry. *J. Vac. Sci. Technol. A* **1994,** *12,* 405–410.
18. Wong, S. C. C.; Lockyer, N. P.; Vickerman, J. C. Mechanisms of Secondary Ion Emission from Self-Assembled Monolayers and Multilayers. *Surf. Interface Anal.* **2005,** *37,* 721–730.
19. Kendall, R. A.; Aprà, E., Bernholdt, D. E.; Bylaska, E. J.; Dupuis, M.; Fann, G. I.; Harrison, R. J.; Ju, J.; Nichols, J. A.; Nieplocha, J.; Straatsma, T. P.; Windus, T. L.; Wong, A. T. High Performance Computational Chemistry: An Overview of NWChem, a Distributed Parallel Application. *Comput. Phys. Commun.* **2000,** *128,* 260–283.
20. Straatsma, T. P.; Aprà, E.; Windus, T. L.; Dupuis, M.; Bylaska, E. J.; de Jong, W.; Hirata, S.; Smith, D. M. A.; Hackler, M.; Pollack, L.; Harrison, R.; Nieplocha, J.; Tipparaju, V.; Krishnan, M., Brown, E.; Cisneros, G.; Fann, G.; Fruchtl, H.; Garza, J.; Hirao, K.; Kendall, R.; Nichols, J.; Tsemekhman, K.; Valiev, M.; Wolinski, K.; Anchell, J.; Bernholdt, D.; Borowski, P.; Clark, T.; Clerc, D.; Daschel, H.; Deegan, M.; Dyall, K.; Elwood, D.; Glendening, E.; Gutowski, M.; Hess, A.; Jaffe, J.; Johnson, B.; Ju, J.; Kobayashi, R.; Kutteh, R.; Lin, Z.; Littlefield, R.; Long, X.; Meng, B.; Nakajima, T.; Niu, S.; Rosing, M.; Sandrone, G.; Stave, M.; Taylor, H.; Thomas, G.; van Lenthe, J.; Wong, A.; Zhang, Z. NWChem, a Computational Chemistry Package for Parallel Computers. Pacific Northwest National Laboratory: Richland, WA; 2003.
21. Perdew, J. P.; Chevary, J. A.; Vosko, S. H.; Jackson, K. A.; Pederson, M. R.; Singh, D. J.; Fiolhais, C. Atoms, Molecules, Solids, and Surfaces: Applications of the Generalized Gradient Approximation for Exchange and Correlation. *Phys. Rev. B* **1992,** *46,* 6671–6687.
22. Dunning, T. H., Jr. Gaussian Basis Sets for Use in Correlated Molecular Calculations. I. The Atoms Boron Through Neon and Hydrogen. *J. Chem. Phys.* **1989,** *90,* 1007–1023.
23. Woon, D. E.; Dunning, T. H., Jr. Gaussian Basis Sets for Use in Correlated Molecular Calculations. III. The Atoms Aluminum through Argon. *J. Chem. Phys.* **1993,** *98,* 1358–1371.
24. Woon, D. E.; Dunning, T. H., Jr. Gaussian Basis Sets for Use in Correlated Molecular Calculations. IV. Calculation of Static Electrical Response Properties. *J. Chem. Phys.* **1994,** *100,* 2975–2988.
25. Koput, J.; Peterson, K. A. Ab Initio Potential Energy Surface and Vibrational-Rotational Energy Levels of $X^2\Sigma^+$ CaOH. *J. Phys. Chem. A* **2002,** *106,* 9595–9599.
26. Dunning, T. H., Jr.; Hay, P. J. Gaussian Basis Sets for Molecular Calculations. In *Methods of Electronic Structure Theory* Vol. III; Schaefer, H. F., III, Ed.; Plenum Press: New York, pp. 1–27.
27. Pacios, L. F.; Christiansen, P. A. Ab Initio Effective Potentials with Spin-Orbit Operators. I. Li Through Ar. *J. Chem. Phys.* **1985,** *82,* 2664–2671.
28. Hurley, M. M.; Pacios, L. F.; Christiansen, P. A.; Ross, R. B.; Ermler, W. C. Ab Initio Effective Potentials with Spin-Orbit Operators. II. K Through Kr. *J. Chem. Phys.* **1986,** *84,* 6840–6853.
29. LaJohn, L. A.; Christiansen, P. A.; Ross, R. B.; Atashroo, T.; Ermler, W. C. Ab Initio Effective Potentials with Spin-Orbit Operators. III. Rb Through Xe. *J. Chem. Phys.* **1987,** *87,* 2812–2824, .
30. Ross, R. B.; Powers, J. M.; Atashroo, T.; Ermler, W. C.; LaJohn, L. A.; Christiansen, P. A. Ab Initio Relative Effective Potentials with Spin-Orbit Operators. IV. Cs through Rn. *J. Chem. Phys.* **1990,** *93,* 6654–6670.
31. Ermler, W. C.; Ross, R. B.; Christiansen, P. A. Ab Initio Relative Effective Potentials with Spin-Orbit Operators. VI. Fr. through Pu. *Int. J. Quantum Chem.* **1991,** *40,* 829–846.
32. Walstedt, R. E.; Bell, R. F. Ionization and Fragmentation of Bi Microclusters by Electron Impact. *Phys. Rev. A* **1986,** *33,* 2830–2832.
33. *CRC Handbook of Chemistry and Physics*, 84th ed.; Lide, D. R., Ed.; CRC Press: 2003.
34. http://webbook.nist.gov/cgi/cbook.cgi?ID=C12595630&Units=SI&Mask=20'#Ion-Energetics, July 9th 2007.

35. Kohl, F. J.; Carlson, K. D. Dissociation Energies of Bismuth-Antimony Molecules. *J. Am. Chem. Soc.* **1968,** *90,* 4814–4817.
36. Cheng, P. Y.; Willey, K. F.; Salicido, J. E.; Duncan, M. A. Resonance-Enhanced Photodissociation Spectroscopy of Mass-Selected Metal Cluster Cations. *Int. J. Mass Spectrom. Ion Processes* **1990,** *102,* 67–80.
37. Hay, P. J.; Wadt, W. R. Ab Initio Effective Core Potentials for Molecular Calculations. Potentials for the Transition Metal Atoms. Sc to Hg. *J. Chem. Phys.* **1985,** *82,* 270–283.
38. Wadt, W. R.; Hay, P. J. Ab Initio Effective Core Potentials for Molecular Calculations. Potentials for Main Group Elements Na to Bi. *J. Chem. Phys.* **1985,** *82,* 284–298.
39. Hay, P. J.; Wadt, W. R. Ab Initio Effective Core Potentials for Molecular Calculations. Potentials for K to Au Including the Outermost Core Orbitals. *J. Chem. Phys.* **1985,** *82,* 299–310.
40. Cotton, F. A.; Wilkinson, G.; Murillo, C. A.; Bochmann, M. Advanced Inorganic Chemistry, 6th ed.; John Wiley Sons, Inc.: New York, 1999; pp. 380–443; 1084–1107.
41. Naylor, S.; Findeis, F.; Gibson, B. W.; Williams, D. H. An Approach Toward the Complete FAB Analysis of Enzymic Digests of Peptides and Proteins. *J. Am. Chem. Soc.* **1986,** *108,* 6359–6363.
42. McLafferty, F. W.; Tureček, F. *Interpretation of Mass Spectra*, 4th ed.; University Science Books: Sausalito, CA, 1993; pp. 238–239.